energy&fuels

pubs.acs.org/EF Article

Effects of Milling and UV Pretreatment on the Pyrolytic Behavior and Thermal Stability of Softwood and Hardwood

Marco Mattonai,* Federica Nardella, Luca Zaccaroni, and Erika Ribechini

Cite This: *Energy Fuels* 2021, 35, 11353−11365 Read Online

ACCESS | Metrics & More | Article Recommendations | Supporting Information

ABSTRACT: UV/visible light is a promising radiation source for biomass pretreatment, but very little knowledge is available on the effect of UV on the thermal behavior of lignocellulose in comparison with more classical, physical pretreatment methods. In this paper, we investigate the effects of ball-milling and UV irradiation on two species of softwood and two species of hardwood, using X-ray diffractometry (XRD), evolved gas analysis-mass spectrometry (EGA-MS), and pyrolysis-gas chromatography coupled to mass spectrometry (Py-GC/MS). The XRD data showed that the crystalline fraction of cellulose was destroyed by milling, but not by irradiation. The EGA-MS data and isoconversional kinetic analysis showed that both milling and irradiation can reduce the thermal stability of wood up to a limit value. The Py-GC/MS data showed that irradiation caused the most significant changes in the pyrolytic behavior of the wood species, increasing the ratio of holocellulose to lignin pyrolysis products and the reactivity of cellulose toward the derivatizing agent. Softwoods were more affected by irradiation than hardwoods. This paper shows that UV irradiation can decrease the recalcitrance of biomass toward pyrolysis, but its efficiency is highly dependent on the type of lignocellulosic substrate.

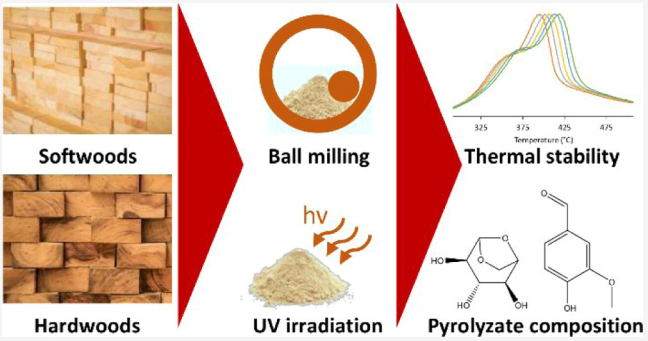

1. INTRODUCTION

Biomass conversion strategies through thermochemical methods have been widely investigated in the last century with the aim of improving the performances of the resulting biofuels[1−3] or the yield of specific valuable chemicals.[4,5] One of the main challenges that must be faced in these conversion processes is the recalcitrance of biomass, which is due to a combination of the entanglement of the holocellulose and lignin fractions, the crystalline domains of cellulose, and the presence of lignin−carbohydrate complexes (LCCs).[6−9] Several pretreatment techniques have been investigated to improve the overall pyrolytic yield of biomass and direct the mechanism toward the formation of specific, desirable products.[10,11] The most traditional pretreatments are based on wet chemistry, using acid, alkaline, or oxidating agents to cleave the chemical bonds in lignocellulose.[12] The main issue of these methods is their low sustainability, as they generate large amounts of wastes and spent chemicals.[13]

Therefore, the attention of the scientific community has turned to alternative pretreatment strategies, mostly based on physical and physicochemical methods.[14,15] Among the physical methods, mechanical pretreatments such as milling, grinding, and extrusion have been considered. Liu and co-workers[16] showed that ball-milling can increase the surface area and the amount of water-soluble carbohydrates of corn stover. Wang and co-workers observed a decrease in the thermal stability of cellulose from cedar and beech after ball-milling.[17] In a previous study by us,[6] we observed that isoconversional methods can be used to track the decrease in thermal stability of cellulose after ball-milling. The application of this strategy to whole lignocellulose could be interesting, but has not been explored yet in the literature.

Irradiation techniques have been recently investigated as an alternative pretreatment strategy capable of cleaving specific bonds and increasing the reactivity of lignocellulose.[15] Typical irradiation techniques are based on microwaves,[14] which favor localized heating of the substrate and the cleavage of the rigid lignocellulose matrix. Pretreatments with other radiation sources such as ultrasound, electron beams, and γ-rays have also been tested.[10,18,19] Ultraviolet (UV) and visible light could constitute another possible radiation source for biomass pretreatment, as UV radiation is known to be the main natural cause for wood degradation.[20,21] UV absorption in wood is mainly due to the lignin fraction,[22,23] and could constitute a possible strategy to increase the accessibility of holocellulose for both thermochemical and biochemical processes. However,

Received: April 6, 2021
Revised: June 18, 2021
Published: July 1, 2021

very few studies have investigated the effects of UV irradiation on the thermal behavior of wood.[20] Due to their high operational costs,[24] the optimization of pretreatment strategies is still an open challenge, and further research is required to both understand the mechanisms at the basis of established pretreatment techniques and to develop optimized, innovative strategies.

Analytical pyrolysis-based techniques such as pyrolysis-gas chromatography coupled with mass spectrometry (Py-GC/MS) have been used extensively to emulate pyrolysis processes on a laboratory scale, in order to improve our knowledge on the thermal degradation mechanism of biomass and evaluate optimization and upgrading strategies.[1,25−28] Py-GC/MS experiments can also be supported by evolved gas analysis-mass spectrometry (EGA-MS), which provides valuable information on the thermal stability and complexity of the investigated materials.[29,30]

In the present work, we investigate the effects on woody biomass of a common pretreatment method, ball-milling, and of a still largely unexplored source for biomass modification, UV light. Changes in crystallinity and pyrolytic behavior are observed for two softwoods (pine and fir) and two hardwoods (oak and chestnut) using X-ray diffractometry (XRD), EGA-MS, and Py-GC/MS with in situ derivatization. Model-free isoconversional methods are also used to estimate apparent activation energies for the thermal degradation of the wood species before and after the pretreatments, and semi-quantitative calculations are carried out on the Py-GC/MS data to evaluate changes in the composition and structure of wood components on a molecular level. This paper provides a first comparative look on the energetics and thermochemical aspects of UV pretreatment of wood, in comparison with a more common pretreatment strategy. To the best of our knowledge, this is the first paper evaluating the effect of physical and physicochemical pretreatments on the thermal stability of wood using EGA-MS and model-free isoconversional methods.

2. MATERIALS AND METHODS

2.1. Samples and Sample Pretreatments. Fir, pine, chestnut, and oak wood were provided by a local supplier as untreated slabs. Sawdust was obtained from the slabs using a drill, and the sawdust was pulverized using a Pulverisette 23 laboratory scale vibratory ball mill (Fritsch, Germany). The ball mill was operated at 50 Hz at room temperature for the minimum amount of time required to obtain a homogeneous powder (approximately 5 min). Wood powders were dried in an oven at 80 °C for 4 h before use. The ash content of the samples was measured by heating a known amount of each wood at 700 °C for 4 h and weighting the residue. The ash content was: fir 0.7%, pine 1.7%, chestnut 0.7%, and oak 1.3%.

Milled wood samples were prepared by weighting 250 mg of each wood in the ball mill and milling for 4 h. The milling time was chosen to ensure a quantitative destruction of the crystalline phase of cellulose, according to a previous study by us.[6] UV-irradiated samples were prepared by weighting 250 mg of each wood inside quartz vessels, which were then sealed and put inside a SOLARBOX 3000 weathering chamber (Co.Fo.Me.Gra., Italy) equipped with a 2500 W xenon lamp. UV irradiation was performed for 28 days at 60 °C and with an irradiance of 800 W/m^2.

2.2. X-ray Diffractometry. XRD experiments were performed with a D2-PHASER spectrometer (Bruker, USA) equipped with a Cu Kα source emitting at 1.54 Å. Spectra were recorded in the range 2θ = 4−60°, with a resolution of 0.016°. Cumulative spectra were obtained by registering three diffractograms for each sample.

2.3. Evolved Gas Analysis-Mass Spectrometry. EGA-MS analyses were carried out using an EGA/PY-3030D microfurnace pyrolyzer (Frontier Laboratories Ltd., Japan) coupled to a 6890 gas chromatograph and a 5973N mass spectrometric detector (Agilent Technologies, USA). In each experiment, the temperature of the furnace was raised from 100 to 700 °C at six different heating rates (15, 20, 25 30, 35, and 40 °C/min). The interface of the pyrolyzer was kept at 100 °C above the furnace temperature, up to a maximum of 300 °C. The GC injector was operated in split mode with a 50:1 ratio at 300 °C. The GC oven and MS transfer-line were kept at 300 °C. The GC injector was directly connected to the MS detector using an UADTM-2.5N deactivated stainless steel capillary tube (3 m × 0.15 mm, Frontier Laboratories Ltd., Japan). Helium (1 mL min^{-1}) was used as carrier gas. The mass spectrometer was operated in EI positive mode (70 eV, m/z range 50−300). The ion source and quadrupole temperatures were 230 and 150 °C, respectively. Approximately 75 μg of sample was used in each experiment.

2.4. Pyrolysis-Gas Chromatography Coupled with Mass Spectrometry. Py-GC/MS analyses were performed with the same instrumentation used for the EGA-MS experiments. Pyrolysis was performed at 550 °C, and the interface temperature was 280 °C. Injection was performed at 280 °C with a 10:1 split ratio. Separation of the pyrolysis products was achieved using an HP-5MS fused silica capillary column (30 m × 0.25 mm, film thickness 0.25 μm, Agilent Technologies, USA) and helium (1 mL min^{-1}) as a carrier gas. The GC oven temperature was raised according to the following program: 50 °C isothermal for 1 min; 10 °C min^{-1} up to 100 °C, then isothermal for 2 min; 4 °C min^{-1} up to 190 °C, then isothermal for 1 min; and 30 °C min^{-1} up to 280 °C, then isothermal for 20 min. The transfer-line to the mass spectrometer was kept at 280 °C. The mass spectrometer was operated in EI positive mode (70 eV, m/z range 50−600) with the same temperatures of the EGA-MS experiments. Approximately 100 μg of sample were used in each experiment. Hexamethyldisilazane (HMDS, 2 μL, Merck, Germany) was used as the derivatizing agent.

2.5. Data Processing. XRD spectra were processed with DIFFRAC (Bruker, USA) and PeakFit (Systat Software Inc., USA). Crystallinity indices (CIs) were calculated for all samples using the spectra deconvolution method.[31] The position of the diffraction peaks of crystalline cellulose was determined using simulated diffraction patterns reported in refs 6 and 32. The deconvolution was performed after subtraction of the background, assuming that the diffraction peaks of both the crystalline and amorphous phases had a Gaussian shape. Once the peak areas were calculated, the CIs were determined using eq 1, in which A_{AM} is the peak area of the amorphous phase and A_{TOT} is the total area of all peaks. The size of crystalline domains was also calculated using the Scherrer eq 2, in which λ is the wavelength of incident light, θ is the angle of the diffraction peak, and b is the peak width at half height.[33]

Thermograms and pyrograms were processed with both MSD ChemStation (Agilent Technologies, USA) and AMDIS (NIST, USA). Thermograms were also processed with isoconversional methods to obtain an estimation of the activation energy of the thermal degradation processes. Isoconversional calculations were performed with MATLAB (v. R2019b), using a script which calculates apparent activation energies using the Kissinger−Akahira−Sunose (KAS), Flynn−Wall−Ozawa, and differential methods. The KAS method provided the best curve fittings for all samples, so it was chosen to discuss the results. The Vyazovkin method was also tested using a macro on Microsoft Excel.[34] The resulting apparent activation energies were within 0.5% of the values obtained with the KAS method.

The ability of the microfurnace pyrolyzer to sustain the selected heating rates was tested with preliminary experiments. The furnace was found capable of maintaining even the highest rate (40 °C min^{-1}) without losing stability. A slight difference between the nominal temperature value and the actual one was observed. This value was proportional to the heating rate, and remained constant throughout the investigated temperature range. For this reason, the actual temperature of the furnace was calculated using eq 3, in which T_0 is

https://doi.org/10.1021/acs.energyfuels.1c01048
Energy Fuels 2021, 35, 11353−11365

the initial temperature, t is the time, β is the heating rate, and −0.129 is the correction factor. The signal $S(T)$ of each thermogram was used to estimate the conversion $\alpha(T)$ using eq 4, in which S_{TOT} is the total integrated area of the thermogram. Apparent activation energies were calculated at fixed values of α from the slope of eq 5, in which E is the activation energy, R the universal gas constant, $p(\alpha)$ the intercept which only depends on α, and T the temperature at which the chosen conversion value was achieved at the given heating rate. For each sample, apparent activation energies were calculated at conversion values 0.2 through 0.7 in 0.1 increments. Activation energies of the holocellulose and lignin fractions were also calculated by extracting pools of m/z signals from the total ion thermograms (TIT) and summing the corresponding extracted ion thermograms, as described in a previous publication.[30] We used the signals at m/z 57, 60, 69, and 73 for holocellulose, m/z 109, 124, 137, and 151 for guaiacyl lignin, and m/z 139, 154, 167, and 181 for syringyl lignin.

Pyrolysis products in the Py-GC/MS profiles were identified based on their mass spectra by comparison with mass spectral libraries (NIST20) and previous publications.[20,35−37] Semiquantitative calculations were performed on the results of Py-GC/MS experiments. First, pyrolysis products were divided into categories based on their structures and mechanisms leading to their formation.[38−41] Categories were classified as holocellulose-specific, lignin-specific, or nonspecific, and as primary or secondary pyrolysis products, as listed in Table 1.

Table 1. Pyrolysis Product Categories and Their Labels

Nonspecific pyrolysis products	
Small molecules	Smo
Hydroxybenzenes	Hyb
Primary holocellulose-specific pyrolysis products	
Monosaccharides	Sug
Anhydrosugars	Ahs
Secondary holocellulose-specific pyrolysis products	
Cyclopentenones	Cyp
Furans	Fur
Pyrans	Pyr
Primary lignin-specific pyrolysis products	
Lignin monomers	Mon
Secondary lignin-specific pyrolysis products	
Phenols	Phe
Shortened alkyl chain	Cha
Demethylated/demethoxylated	Dem
Oxidized	Oxd

Then, the peaks belonging to identified compounds were integrated in all pyrograms. The ratio of holocellulose-to lignin-specific pyrolysis products (H/L) was calculated for each sample to obtain an estimation of the relative amounts of the two fractions of wood both before and after the pretreatments.[37,42]

$$CI = 1 - A_{AM}/A_{TOT} \quad (1)$$

$$\tau = \lambda/b \cos\theta \quad (2)$$

$$T = T_0 + (t - 0.129)\beta \quad (3)$$

$$\alpha(T) = \int_{T_0}^{T} S(\tau)/S_{TOT}\, d\tau \quad (4)$$

$$\ln(\beta/T^2) = -E/RT + p(\alpha) \quad (5)$$

To obtain further insight into the pyrolytic behavior of the samples, total areas were calculated for all categories by adding the areas of all members of each category. Category areas of small molecules and hydroxybenzenes were expressed as percentages of the total area of the pyrogram, while category areas of holocellulose- and lignin-specific pyrolysis products were expressed as percentages of the total area of the fraction-specific compounds. The ratios of secondary to primary pyrolysis products for holocellulose and lignin (S/P_H and S/P_L, respectively) were also calculated using eqs 6 and 7.

Finally, reproducibility of the XRD, EGA-MS, and Py-GC/MS results was evaluated by analyzing replicates. In the case of XRD, relative standard deviations were calculated by repeating the deconvolution process three times on the same sample and were found to be 10% on average. In the case of EGA-MS, relative standard deviations were calculated using the areas of TIT divided by sample weights and were found to be 5% on average. For Py-GC/MS, relative standard deviations were calculated on integrated peak areas expressed as percentages of the total area of identified peaks and were found to be 10% on average.

$$S/P_H = \frac{Cyp + Fur + Pyr}{Ahs + Sug} \quad (6)$$

$$S/P_L = \frac{Phe + Cha + Dem + Oxd}{Mon} \quad (7)$$

3. RESULTS AND DISCUSSION

3.1. XRD. The XRD spectra obtained for all samples are available in the Supporting Information. The observed diffraction patterns can be ascribed to the crystalline fraction of cellulose,[6,31] showing a main diffraction peak around 2θ = 22° corresponding to the (200) diffraction plane, and a double peak around 2θ = 15° corresponding to the (1−10) and (110) diffraction planes. An additional, broad signal can be observed superimposed on the diffraction peaks. This signal can be attributed to the amorphous phase of the sample. Given the shapes of the diffractograms, deconvolution of the spectra was performed assuming that all samples displayed four Gaussian peaks, three for the crystalline phase, and one for the amorphous phase.

The CI and τ values are presented in Table 2, while a comparison between the experimental diffractogram and the deconvoluted peaks is provided in the Supporting Information. All deconvolutions provided r^2 values higher than 0.96.

Table 2. CIs and r^2 Values for the XRD Spectral Deconvolutions of all Wood Samples, and Crystallite Dimensions for Untreated and Irradiated Samples

	CI	r^2 of fit	τ (nm)		CI	r^2 of fit	τ (nm)
FIR				CHESTNUT			
untreated	0.33	0.998	3.2	untreated	0.28	0.992	2.8
milled	0.03	0.979		milled	0.04	0.969	
irradiated	0.33	0.996	3.2	irradiated	0.27	0.991	2.9
PINE				OAK			
untreated	0.33	0.993	3.1	untreated	0.27	0.990	2.9
milled	0.03	0.975		milled	0.04	0.960	
irradiated	0.30	0.998	3.2	irradiated	0.24	0.994	2.9

https://doi.org/10.1021/acs.energyfuels.1c01048
Energy Fuels 2021, 35, 11353−11365

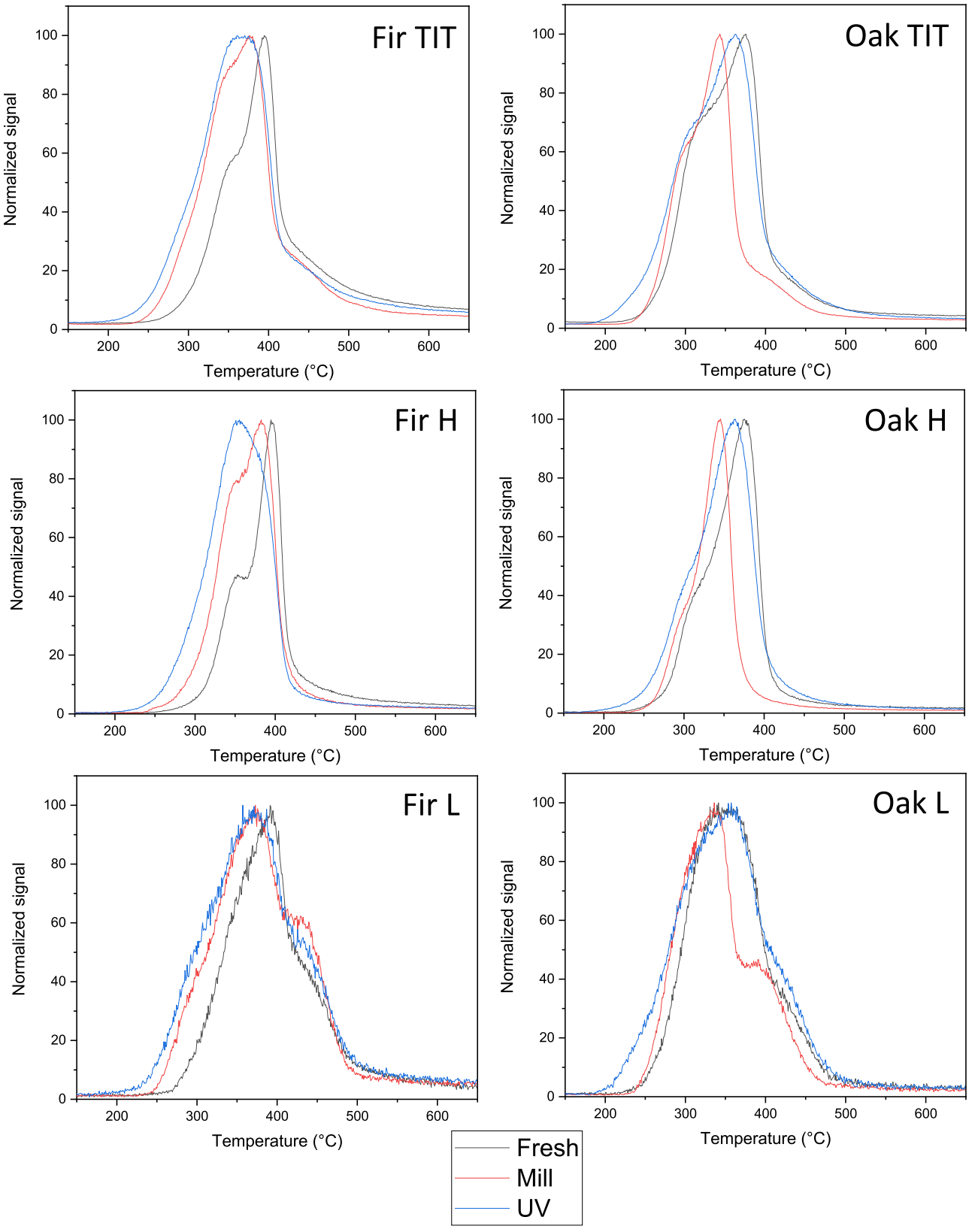

Figure 1. TIT and holocellulose (H) and lignin-specific (L) thermograms for fresh, milled, and irradiated fir and oak (β = 20 °C/min).

Softwood samples showed slightly higher CIs and τ than hardwood samples. This result is unexpected, as softwoods usually contain a higher amount of lignin than hardwoods.[1] A higher lignin content should increase the peak intensity of the amorphous phase, leading to lower CIs.[43] This result indicates that, despite the higher content of holocellulose, the amorphous fraction of the two hardwoods generates a comparable peak intensity to that of softwoods. This could be due to a higher content of hemicellulose, a higher content of amorphous cellulose, or both.

https://doi.org/10.1021/acs.energyfuels.1c01048
Energy Fuels 2021, 35, 11353−11365

Table 3. Onset and Peak Temperatures for the TITs of all Samples (β = 20 °C/min)[a]

		FIR			PINE			CHESTNUT			OAK		
temperature (°C)		fresh	mill	UV	fresh	mill	UV	fresh	mill	UV	fresh	mill	UV
TIT	onset	275	251	227	257	235	233	251	251	235	246	246	210
	peak	395	376	361	390	374	375	333	314	329	375	343	362
H	onset	301	273	249	270	233	249	261	257	246	267	264	239
	peak	395	383	355	396	375	381	335	316	330	376	346	364
L	onset	276	251	232	265	246	227	246	253	224	247	244	212
	peak	391	373	357	387	365	373	334	318	331	341	336	357

[a]The onset temperature has been determined as the temperature at which the signal intensity of each thermogram reaches 5% of the peak.

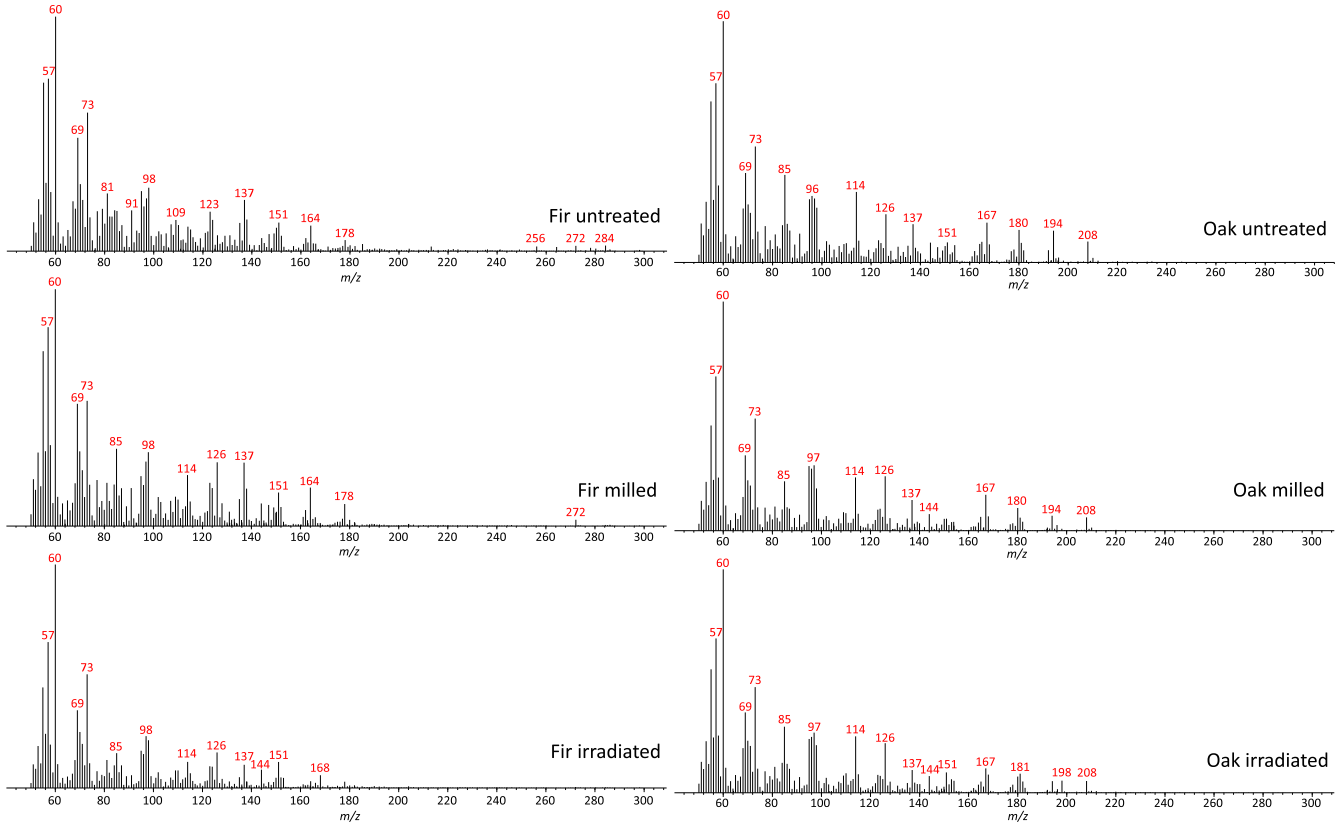

Figure 2. Average mass spectra from the EGA-MS profiles of fresh, milled, and irradiated fir and oak (β = 20 °C/min).

As expected, the milled samples showed an almost totally amorphous cellulose, in agreement with the literature.[16] On the contrary, no significant variation was observed for irradiated samples, as their CIs were within the experimental error of the untreated ones. Table 2 also presents the crystallite size estimated with the Scherrer equation for untreated and irradiated samples. The crystallite size could not be calculated for the milled samples, due to the high background noise of amorphous cellulose. As for the CIs, no significant variation in the crystallite size was observed between the untreated and irradiated samples.

3.2. EGA-MS. The thermograms obtained at β = 20 °C/min for fir and oak wood, representative of a softwood and a hardwood species, respectively, are presented in Figure 1, while those obtained for the other samples are available in the Supporting Information. The total ion profiles of the untreated wood samples were similar to those available in the literature, with a main peak around 390−400 °C corresponding to the degradation of cellulose, a shoulder peak in the range 300−350 °C corresponding to the degradation of hemicellulose and the primary pyrolysis of lignin, and a second, lower shoulder peak beyond 400 °C that can be ascribed to secondary pyrolysis of lignin and the formation of aromatic compounds.[44] The relative height of the hemicellulose shoulder peak is different for the four wood species, suggesting that they contain different amounts of hemicellulose. In particular, fir and chestnut show a lower hemicellulose content than pine and oak. However, the CIs of the two softwoods were very similar, as were those of the two hardwoods. This leads us to conclude that fir and chestnut contain a higher amount of amorphous cellulose than pine and oak, respectively. Holocellulose- and lignin-specific thermograms are also displayed in Figure 1. The extracted thermograms highlight the thermal degradation regions of the two fractions of wood, showing both the double peak of hemicellulose and cellulose, and the two-step degradation profile of lignin.

Both ball-milling and UV irradiation caused notable changes in the shape of the thermal degradation profiles. This change mainly consisted in the coalescence of the thermal degradation peaks of hemicellulose and cellulose, as can be observed from

https://doi.org/10.1021/acs.energyfuels.1c01048
Energy Fuels 2021, 35, 11353−11365

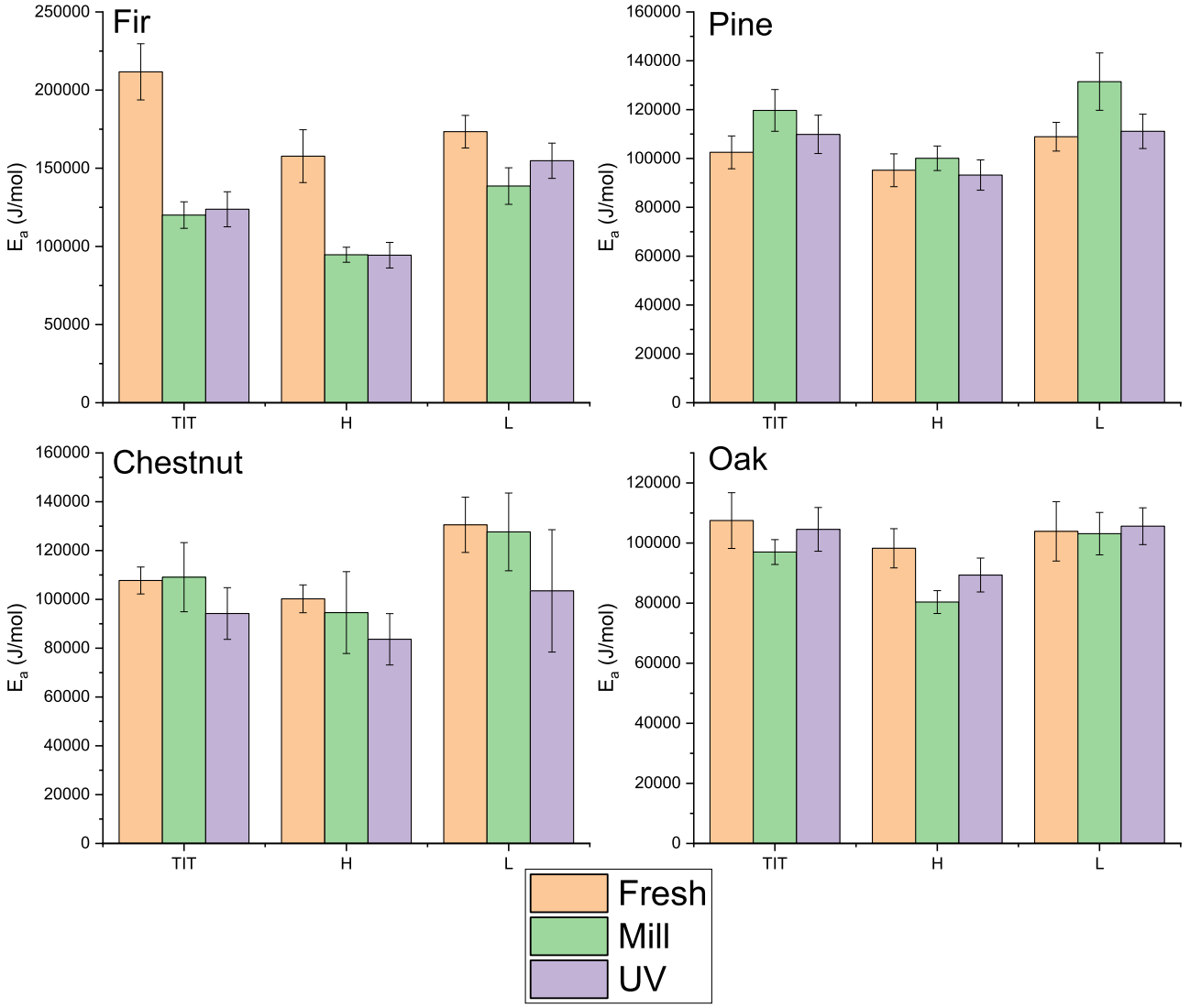

Figure 3. Apparent activation energies obtained from model-free isoconversional elaboration of TIT, and holocellulose (H) and lignin-specific (L) thermograms of all samples.

the holocellulose-specific thermograms. The coalescence was particularly evident for all wood samples after milling. This result can be ascribed to the cleavage of the crystalline phase of cellulose,[16] which reduces its thermal stability. On the other hand, the coalescence of peaks after irradiation was only observed for the two softwoods. This is not related to the loss of crystallinity, as the XRD results show no decrease in the CIs of irradiated samples, but rather to a degradation of the amorphous phase of holocellulose. This result was already observed in a previous study.[20] Regarding lignin, changes in the thermal degradation profiles were less significant, suggesting that milling and irradiation had little effect on its thermal degradation process.

A shift of both the onset and the signal peak temperatures to lower values was observed for all milled and irradiated samples. This indicates that even if the pyrolysis mechanisms were not significantly altered, both lignin and holocellulose underwent some form of degradation after milling and irradiation. The offset temperatures were also slightly shifted at lower values for the treated samples, but these shifts were less significant than those of the onset temperatures, resulting in a general broadening of all the thermal degradation profiles toward the lower temperature values. This suggests that a fraction of all wood samples retained the original thermal stability. The temperatures corresponding to the signal onsets and the signal peaks for all samples are listed in Table 3. As already observed, softwoods were more affected than hardwoods by both milling and UV irradiation. Fir was the wood species with the most significant variations, showing a shift in the peak onset of approximately 50 °C after irradiation. It is also interesting to notice that the peak temperatures for hardwoods decreased by a larger extent after milling than after degradation, while the shifts for softwoods were very similar. This is related to the higher holocellulose content and lower lignin content of hardwoods compared to softwoods, which increased the overall observed effect of milling on the shape of the thermograms of hardwoods.

Further insights into the alteration of the lignin fraction can be obtained from the average mass spectra of the thermograms, which are shown in Figure 2 for fir and oak, and in the Supporting Information for the other samples. These spectra were obtained by averaging the mass spectra of all points of the thermograms between the signal onsets and offsets. Structures for some of the ions corresponding to the main m/z values in

https://doi.org/10.1021/acs.energyfuels.1c01048
Energy Fuels 2021, 35, 11353−11365

Table 4. Identified Compounds in the Pyrograms of all Samples[a]

#	RT (min)	name	org	cat	*m*/z
1	8.9	1,2-dihydroxyethane (2TMS)		Smo	191, 147, 103, 73
2	9.2	2-hydroxymethylfuran (TMS)	H	Fur	170, 155, 81
3	9.6	*trans*-1,2-dihydroxyethylene (2TMS)		Smo	204, 189, 73
4	10.7	phenol (TMS)		Hyb	166, 151
5	10.9	2-hydroxypropanoic acid (2TMS)		Smo	219, 191, 147, 117, 73
6	11.2	2-furancarboxylic acid (TMS)	H	Fur	184, 169, 125, 95
7	11.3	hydroxyacetic acid (2TMS)		Smo	220, 205, 161, 147, 73
8	11.4	4-hydroxy-2-butenal (TMS)		Smo	158, 143, 130, 103, 73
9	11.8	guaiacol	L	Cha	124, 109, 81
10	12.3	3-hydroxypropanone, enolic form (2TMS)		Smo	217, 191, 147, 73
11	12.3	3-hydroxymethylfuran (TMS)	H	Fur	170, 155, 81
12	12.9	*o*-cresol (TMS)	L	Phe	180, 165, 135, 91
13	13.2	*m*-cresol (TMS)	L	Phe	180, 165
14	13.2	*p*-cresol (TMS)	L	Phe	180, 165, 91
15	13.3	2-hydroxy-5-methylfuran (TMS)	H	Fur	170, 155, 111, 81
16	13.3	3-hydroxypropanoic acid (2TMS)		Smo	219, 177, 147, 73
17	13.9	3-hydroxy-(4*H*)-pyran-4-one (TMS)	H	Pyr	184, 169, 95, 73
18	14.0	2-hydroxy-(4*H*)-pyran-4-one (TMS)	H	Pyr	184, 169, 95
19	14.7	2-hydroxycyclopenta-1,3-dione (TMS)	H	Cyp	171, 143, 101, 75, 73
20	15.1	1,2-dihydroxybenzene (TMS)		Hyb	182, 167, 151, 91, 73
21	15.3	5-hydroxy-2*H*-pyran-4(3*H*)-one (TMS)	H	Pyr	186, 171, 143, 129, 101, 75
22	15.3	2-hydroxymethyl-3-methylcyclopentenone (TMS)	H	Cyp	198, 183, 73
23	15.6	2-methylcyclopenta-1,3-dione, enolic form (TMS)	H	Cyp	184, 169, 139, 117, 73
24	15.8	1,3-dihydroxyacetone (2TMS)		Smo	219, 189, 147, 103, 73
25	15.9	guaiacol (TMS)	L	Cha	196, 181, 166, 151, 103, 73
26	17.6	glycerol (3TMS)		Smo	218, 205, 147, 133, 117, 103, 73
27	17.3	*Z*-2-penten-1-ol (TMS)		Oth	158, 143, 129, 73
28	17.4	3-hydroxy-6-methyl-(2*H*)-pyran-2-one(TMS)	H	Pyr	198, 183, 168
29	18.0	2,3-dihydrofuran-2,3-diol (2TMS)	H	Fur	246, 231, 147, 73
30	18.0	4-hydroxymethylphenol (TMS)		Hyb	196, 180, 165, 149, 105, 75
31	18.0	3-hydroxymethylphenol (TMS)		Hyb	196, 180, 165, 149, 105, 75
32	18.6	5-hydroxymethyl-2-furaldehyde (TMS)	H	Fur	198, 183, 169, 109, 73, 53
33	18.6	4-vinylguaiacol	L	Cha	150, 135, 107, 77
34	18.8	4-methylguaiacol (TMS)	L	Cha	210, 195, 180, 73
35	18.8	1,2-dihydroxybenzene (2TMS)		Hyb	254, 239, 151, 73
36	19.3	3-hydroxycyclopenta-1,2-dione, enolic form (2TMS)	H	Cyp	258, 243, 230, 169, 147, 73
37	19.4	2,3-dihydroxypropanoic acid (3TMS)		Smo	307, 292, 205, 189, 147, 133, 103, 73
38	19.6	1:4,3:6-anhydro-α-D-glucopyranose (TMS)	H	Ahs	170, 155, 145, 129, 103, 81, 73
39	20.0	eugenol	L	Cha	164, 149, 131, 121, 103, 91, 77, 65, 55
40	20.6	2-hydroxymethyl-3-hydroxytetrahydropyran (2TMS)	H	Pyr	217, 191, 147, 129, 103, 73
41	21.1	4-methylcatechol (2TMS)	L	Dem	268, 253, 180, 73
42	21.2	4-ethylguaiacol (TMS)	L	Cha	224, 209, 194, 179
43	21.4	syringol (TMS)	L	Cha	226, 211, 196, 181
44	21.4	1,4-dihydroxybenzene (2TMS)		Hyb	254, 239, 147, 73
45	21.6	5-formyltetrahydrofuran-2-carboxylic acid (TMS)	H	Fur	173, 143, 129, 73
46	21.7	arabinofuranose (4TMS)	H	Sug	230, 217, 147, 129, 73
47	21.9	2-(1,2-dihydroxyethyl)furan (2TMS)	H	Fur	272, 257, 183, 169, 147, 73
48	22.5	4-vinylguaiacol (TMS)	L	Cha	222, 207, 192, 177, 162
49	22.7	3-hydroxy-2-hydroxymethyl-2-cyclopentenone (2TMS)	H	Cyp	272, 257, 147, 73
50	22.8	2-hydroxycyclopenta-1,3-dione, enolic form (2TMS)	H	Cyp	243, 73
51	22.8	3-deoxypentofuranose (3TMS)	H	Fur	157, 155, 147, 129, 103, 73
52	23.0	3,5-dihydroxy-2-methyldihydro-(4*H*)-pyran-4-one (2TMS)	H	Pyr	288, 273, 245, 217, 183, 155, 147, 133, 101, 73
53	23.2	methylhydroquinone (2TMS)		Oth	282, 268, 253, 237, 179, 163, 119, 73
54	23.3	4-ethylcatechol (2TMS)	L	Dem	282, 267, 193, 179, 73
55	23.5	3-hydroxy-2-hydroxymethylcyclopenta-2,4-dienone (2TMS)	H	Cyp	270, 255, 133, 73
56	23.5	eugenol (TMS)	L	Cha	236, 221, 206, 179
57	23.9	4-methylsyringol (TMS)	L	Cha	240, 225, 210, 195, 167
58	24.0	3-methoxy-1,2-benzenediol (2TMS)	L	Dem	284, 269, 254, 239, 196, 169, 153
59	24.0	3,5-dihydroxy-2-methyl-(4*H*)-pyran-4-one (2TMS)	H	Pyr	271, 199, 128, 73
60	24.3	1,6-anhydro-β-D-glucopyranose (TMS C4)	H	Ahs	155, 145, 129, 103, 73
61	24.5	4-hydroxy-5-oxopentanoic acid (2TMS)		Oth	276, 261, 233, 147, 129, 117, 103, 73

https://doi.org/10.1021/acs.energyfuels.1c01048
Energy Fuels 2021, 35, 11353−11365

Table 4. continued

#	RT (min)	name	org	cat	*m*/*z*
62	24.6	1,6-anhydro-*β*-D-glucopyranose (TMS C2)	H	Ahs	155, 145, 129, 116, 101, 73
63	25.0	*E*-isoeugenol (TMS)	L	Cha	236, 221, 206, 179, 73
64	25.1	3-hydroxy-5-oxopentanoic acid (2TMS)		Oth	276, 261, 233, 147, 129, 117, 103, 73
65	25.4	vanillin (TMS)	L	Oxd	224, 209, 194
66	25.5	2-methyl-3-hydroxycyclopentanone, enolic form (2TMS)	H	Cyp	258, 243, 185, 147, 103, 73
67	25.7	1,4-dihydroxy-2-methoxybenzene (2TMS)	L	Dem	284, 269, 254, 239, 73
68	25.8	5-methyl-3-methoxy-1,2-benzenediol (2TMS)	L	Dem	298, 283, 268, 253, 210, 167, 73
69	25.8	1,2,3-trihydroxybenzene (3TMS)		Hyb	342, 327, 239, 73
70	26.0	4-ethylsyringol (TMS)	L	Cha	254, 239, 224, 209
71	26.4	*Z*-isoeugenol (TMS)	L	Cha	236, 221, 206
72	26.7	1,4-anhydro-D-galactopyranose (2TMS)	H	Ahs	147, 145, 129, 116, 103, 73
73	26.8	1,6-anhydro-D-galactopyranose (2TMS)	H	Ahs	204, 189, 161, 145, 129, 101, 73
74	27.1	2-hydroxymethyl-5-hydroxy-2,3-dihydro-(4*H*)-pyran-4-one (2TMS)	H	Pyr	288, 273, 183, 155, 147, 129, 73
75	27.3	4-vinylsyringol (TMS)	L	Cha	252, 237, 222, 179, 73
76	27.5	1,2,4-trihydroxybenzene (3TMS)		Hyb	342, 327, 239, 73
77	27.6	1,4-anhydro-*β*-D-glucopyranose (2TMS)	H	Ahs	217, 157, 145, 129, 103, 73
78	27.6	5-hydroxy-6-oxohexanoic acid (2TMS)		Oth	290, 275, 247, 203, 157, 147, 129, 116, 101, 75, 73
79	27.9	acetovanillone (TMS)	L	Oxd	238, 223, 208, 193
80	28.1	1,6-anhydro-*β*-D-glucofuranose (2TMS)	H	Ahs	294, 217, 204, 191, 155, 129, 116, 101, 73
81	28.2	1,6-anhydro-*β*-D-glucopyranose (2TMS)	H	Ahs	217, 204, 191, 147, 129, 116, 101, 73
82	29.0	4-hydroxy-3,5-dimethoxycinnamic acid methyl ester (TMS)	L	Oxd	310, 295, 280, 265, 250, 222, 179, 133
83	29.9	1,6-anhydro-*β*-D-glucopyranose isomer (3TMS)	H	Ahs	333, 217, 204, 191, 129, 103, 73
84	30.1	syringaldehyde (TMS)	L	Oxd	254, 239, 224, 73
85	30.4	2,3,5-trihydroxy-(4*H*)-pyran-4-one (3TMS)	H	Pyr	360, 345, 330, 270, 255, 147, 133, 103, 73
86	30.5	1,6-anhydro-*β*-D-glucopyranose (3TMS)	H	Ahs	333, 217, 204, 147, 129, 73
87	30.7	1,4-anhydro-*β*-D-glucopyranose (3TMS)	H	Ahs	332, 217, 204, 191, 157, 147, 73
88	30.8	*Z*-propenylsyringol (TMS)	L	Cha	266, 251, 236, 205, 73
89	31.5	1,6-anhydro-*β*-D-glucofuranose (3TMS)	H	Ahs	319, 243, 217, 191, 147, 116, 73
90	31.8	vanillic acid (2TMS)	L	Oxd	312, 297, 282, 267, 253, 223, 193, 126, 73
91	32.0	acetosyringone (TMS)	L	Oxd	268, 253, 238, 223, 193
92	32.6	syringic acid methyl ester (TMS)	L	Oxd	284, 269, 254, 223, 73
93	32.8	3-vanillylpropanol (2TMS)	L	Cha	326, 311, 236, 221, 206, 179, 149, 73
94	33.0	*Z*-coniferyl alcohol (TMS)	L	Mon	252, 235, 221, 204, 181, 162, 131, 103, 73
95	33.1	coniferaldehyde (TMS)	L	Oxd	250, 235, 220, 192, 177, 73
96	33.7	syringic acid (2TMS)	L	Oxd	342, 327, 312, 297, 283, 253, 223, 141, 73
97	33.9	gluconic acid *δ*-lactone (4TMS)	H	Sug	332, 305, 217, 204, 189, 147, 129, 103, 73
98	34.1	*E*-Coniferyl alcohol (2TMS)	L	Mon	324, 309, 293, 235, 219, 204, 73
99	34.3	syringylpropanol (2TMS)	L	Cha	356, 341, 326, 266, 253, 240, 236, 210, 163
100	34.3	gallic acid (4TMS)		Oth	458, 443, 355, 281, 179, 147, 73
101	34.3	*Z*-synapyl alcohol (2TMS)	L	Mon	354, 339, 323, 293, 265, 234, 204, 73
102	34.5	3,4-dihydroxycinnamyl alcohol (3TMS)	L	Dem	382, 355, 293, 205, 179, 147, 73
103	34.6	sinapylaldehyde (TMS)	L	Oxd	280, 265, 250, 222, 179, 73
104	35.1	Synapyl alcohol (TMS)	L	Mon	282, 251, 234, 192, 177, 161, 133, 73
105	35.1	*E*-Synapyl alcohol (2TMS)	L	Mon	354, 339, 323, 293, 265, 234, 204, 73

[a]Numbers refer to the peaks in the pyrograms of Figure 4. The retention time (RT), originating polymer (Org), compound category (Cat), and main *m*/*z* signals in the mass spectrum are presented for each compound. The base peak in each mass spectrum is underlined.

these spectra are available in the literature.[30,44] The average mass spectrum of fir after milling showed little variation compared to the untreated one, while the one after irradiation showed a decrease in the signal intensities of the *m*/*z* values related to lignin (137, 151, and 164), indicating a degradation of this fraction due to UV exposure. The average mass spectrum of oak was less affected than that of fir by irradiation, showing similar intensities of the lignin-specific *m*/*z* signals even after UV exposure. This result agrees with the changes observed for the thermograms profiles.

Data from both the total ion and component-specific thermograms were processed using model-free isoconversional methods. The average apparent activation energies obtained are shown in Figure 3, while KAS plots and conversion plots are available in the Supporting Information. It is important to notice that the activation energies obtained from the TITs should not be compared with those of the component-specific thermograms, as they were calculated following different procedures. Fir showed the most significant reduction in apparent activation energy, after both milling and irradiation. This decrease in thermal stability can be mostly ascribed to the holocellulose fraction, as the apparent activation energy of the lignin fraction was less affected by either pretreatment. No significant changes were observed for the other samples. To account for this result, we observed that the absolute value of the apparent activation energy for untreated fir wood was approximately double compared to the other wood species. Given this difference, we concluded that milling and irradiation

https://doi.org/10.1021/acs.energyfuels.1c01048
Energy Fuels 2021, 35, 11353−11365

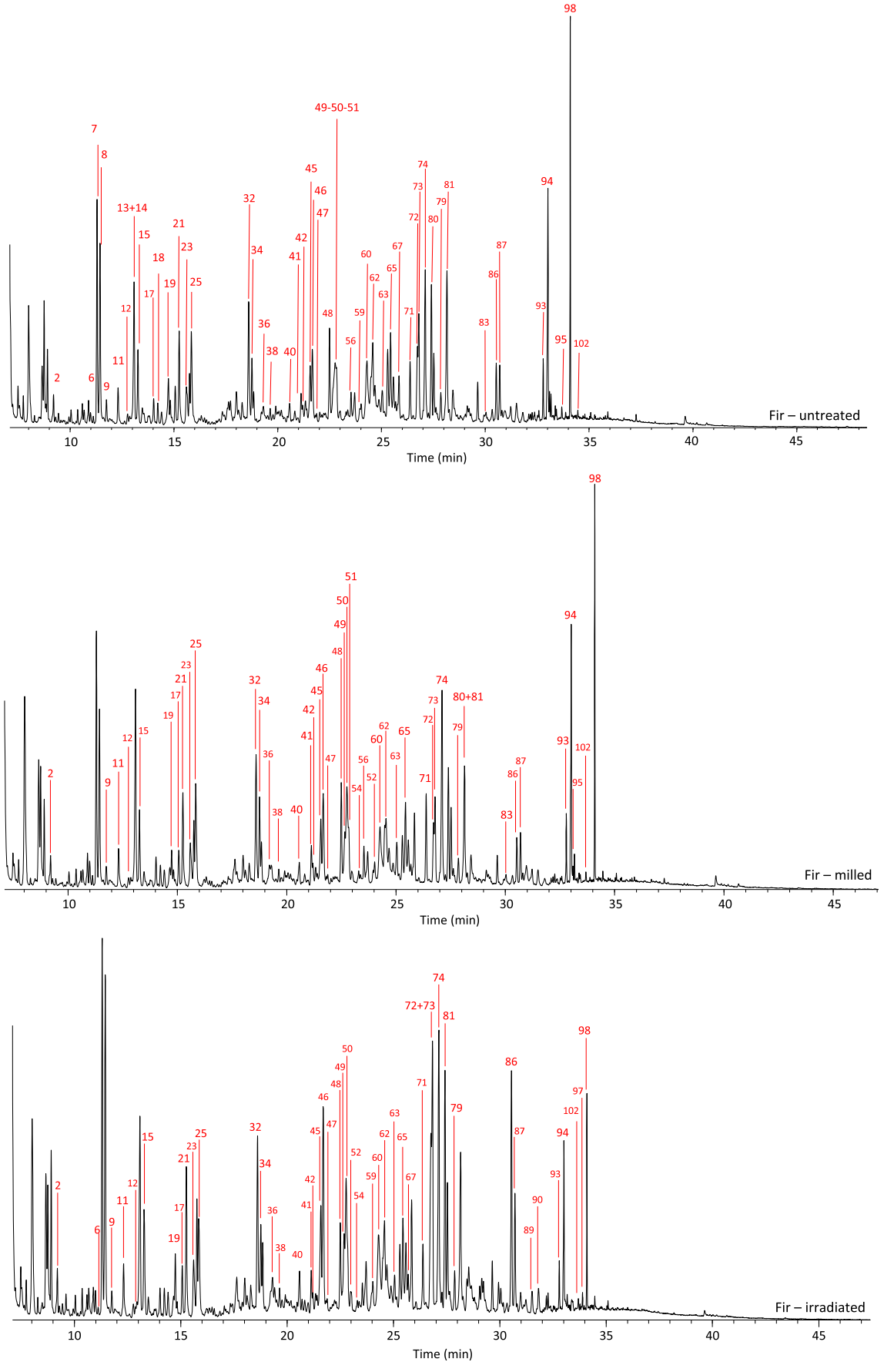

Figure 4. Pyrograms of untreated, milled, and irradiated fir. Peaks are labeled according to Table 4.

https://doi.org/10.1021/acs.energyfuels.1c01048
Energy Fuels 2021, 35, 11353−11365

can only reduce the thermal stability of wood up to a limit value. The thermal stability of fir wood was high enough to be significantly reduced by the two pretreatments, while those of the other wood species were already low and could not be reduced further.

The reason for the different thermal stability of fir compared to the other wood species has not been clearly identified. All four wood species have different compositions of the organic fraction and different contents of inorganic species. Sample composition plays a fundamental role in determining the thermal behavior. However, no specific characteristics can be outlined that differentiate fir from the other wood species. Because the CIs of the untreated wood species were comparable, the difference is not due to different contents in the crystalline phase of cellulose. Differences in the spatial disposition of the crystalline domains could influence the thermal stability of the four wood species. It should be remembered that isoconversional methods only provide an estimation of the activation energy associated with a certain thermal degradation process. Therefore, the values obtained in the present work should not be considered as an absolute limit in the efficacy of ball-milling.

3.3. Py-GC/MS. Table 4 presents a list of identified compounds in the pyrograms of all samples. The pyrograms obtained for untreated, milled, and irradiated fir are presented in Figure 4, while the pyrograms obtained for the other wood species are available in the Supporting Information. The pyrogram of untreated fir was dominated by the peaks of *Z*-coniferyl alcohol (#94) and *E*-coniferyl alcohol (#98), as well as by the peaks of hydroxyacetic acid (#7) and 4-hydroxy-2-butenal (#8). The other untreated wood species provided similar pyrograms. The profile of the pyrogram did not change significantly after milling, confirming that the effect of this pretreatment was mostly physical. On the contrary, significant changes were observed after irradiation. The most striking difference was the reduction of intensity of the peaks belonging to lignin monomers, indicating an extensive degradation of this fraction of wood.

Semiquantitative calculations were performed on the integrated peak areas of identified compounds to evaluate the changes in pyrolytic behavior in more detail. These calculations were possible because all samples provided very similar yields of volatile pyrolysis products. This was confirmed by the negligible amount of solid residue left in the sample cup after pyrolysis. Figure 5 shows the H/L values obtained for all samples. The H/L values were higher for untreated hardwoods than for the softwoods, as softwoods usually have higher lignin contents than hardwoods.[1] A particularly high H/L value was obtained for chestnut, indicating a very high content of holocellulose. This result is consistent with the discussions that were made in the previous sections in light of the CI values and thermogram profiles. Milling did not significantly affect the H/L ratio of fir, pine, and oak wood, while a significant reduction was observed for chestnut. The peculiar behavior of chestnut is likely due to the higher cellulose content. The higher content of cellulose likely led to a more extensive degradation, favoring secondary reactions upon pyrolysis and increasing the yield of small molecules which are not included in the calculation of the H/L.

On the other hand, UV irradiation caused a significant increase in the H/L ratios for all wood species, indicating a reduction in the characteristic pyrolysis products of lignin. This result can be correlated with the partial degradation of lignin

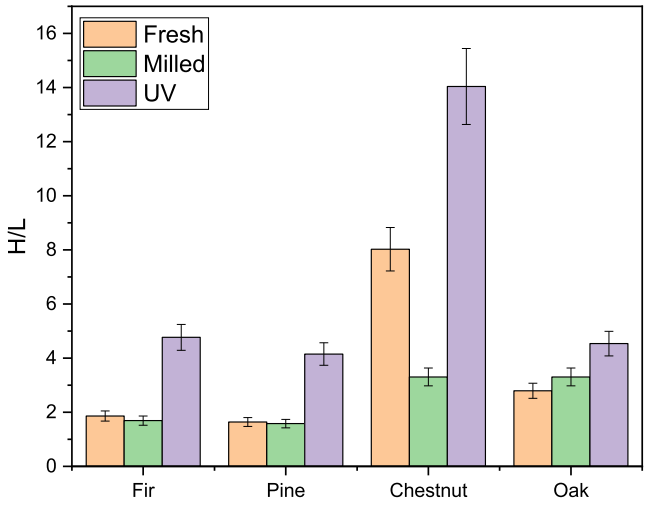

Figure 5. H/L values calculated from the Py-GC/MS data for all analyzed samples.

that was observed from EGA-MS analyses. The reduction in lignin content after irradiation suggests that this pretreatment method could provide a significant advantage in the development of processing technologies for the holocellulose fraction of wood. In fact, lignin can hinder biological and chemical processing of holocellulose.[8,9,45]

Table 5 lists the percentage category areas and the ratios of secondary to primary pyrolysis products for all samples. The percentage areas of small molecules were generally higher for softwoods than for hardwoods, and they were mostly unaffected by the pretreatments. The only exception to this was chestnut, whose areas of small molecules became more than double after milling. This result is consistent with the hypothesis that milling induced a more severe degradation of the holocellulose fraction in chestnut compared to the other woods. On the contrary, the area of small molecules did not increase for any of the irradiated samples, despite the H/L indicating a depletion of the lignin fraction after irradiation. This is due to the release of carbon dioxide from the lignin network during irradiation, which cannot be observed by Py-GC/MS but has been previously described in the literature.[21]

After milling, the S/P_H increased, due to both a decrease in the category area of anhydrosugars, and an increase in that of cyclopentenones, furans, and pyrans. This effect was mainly observed in fir and chestnut. On the other hand, irradiation had an opposite effect, increasing the yields of anhydrosugars, decreasing those of secondary pyrolysis products, and leading to a decrease of the S/P_H. These changes were mainly observed in the two softwoods.

Variations in the yields of pyrolysis products of holocellulose can be ascribed to numerous factors. For instance, it has been shown that the presence of a silylating agent can influence the pyrolytic yields of carbohydrates based on the accessibility of the hydroxy groups. Polysaccharides with more accessible hydroxy groups will generally provide higher yields of anhydrosugars, as the derivatization process will be faster and will hinder secondary pyrolysis.[46] In a previous study, we showed that ball-milling of pure cellulose not only led to a decrease in its CI, but also in its average degree of polymerization.[6] The decrease in anhydrosugars yields after milling observed in the present work indicates that, although the crystalline phase of cellulose was cleaved, the accessibility

https://doi.org/10.1021/acs.energyfuels.1c01048
Energy Fuels 2021, 35, 11353−11365

Table 5. Percentage Category Areas and Ratios of Secondary to Primary Pyrolysis Products From the Py-GC/MS Analysis of all Samples

		FIR			PINE			CHESTNUT			OAK		
		fresh	mill	UV	fresh	mill	UV	fresh	mill	UV	fresh	mill	UV
						percentage of total							
Smo		15.1	16.4	16.9	16.0	17.9	14.7	2.4	5.3	3.6	6.8	5.3	10.4
Hyb		6.2	6.6	6.5	8.1	8.0	6.8	2.2	4.0	2.0	3.7	4.0	4.2
						percentage of fraction							
Cyp	H	11.8	11.5	9.8	13.2	13.8	13.9	10.9	14.4	8.5	12.9	14.4	14.3
Fur	H	20.6	22.5	13.9	28.4	26.0	17.1	2.8	12.3	2.3	10.8	12.3	9.6
Pyr	H	19.8	24.2	17.8	20.6	22.4	18.3	11.3	18.2	8.9	18.0	18.2	17.2
Ahs	H	42.3	33.7	48.2	31.4	30.2	44.2	60.7	46.3	68.4	46.5	46.3	51.2
Sug	H	5.5	8.2	10.4	6.4	7.5	6.6	14.3	8.7	11.9	11.7	8.7	7.8
S/P_H	H	1.1	1.4	0.7	1.7	1.7	1.0	0.3	0.8	0.2	0.7	0.8	0.7
Phe	L	0.7	0.8	0.6	0.6	0.5	0.5	0.3	0.3	0.2	0.4	0.3	0.1
Cha	L	40.8	49.9	42.8	46.4	51.4	37.8	56.2	66.5	44.4	47.3	66.5	43.4
Dem	L	4.4	6.1	8.0	4.0	4.0	6.1	3.8	7.1	6.4	4.9	7.1	6.3
Oxd	L	12.1	9.7	22.7	9.2	9.1	28.0	9.2	7.0	36.0	11.5	7.0	18.7
Mon	L	42.2	33.5	25.8	39.8	35.0	27.5	30.6	19.1	13.0	35.9	19.1	31.4
S/P_L	L	1.4	2.0	2.9	1.5	1.8	2.6	2.3	4.2	6.7	1.8	4.2	2.2

of the hydroxy groups was not affected. The discrepancy between the results observed for pure cellulose and cellulose in wood must, therefore, be attributed to the other components of wood, hemicellulose and lignin. The presence of LCCs in the wood matrix is a likely explanation for this difference. LCCs contain ether and ester bonds between lignin and hemicellulose, and increase the recalcitrance and structural stiffness of wood.[7,47] LCCs are not cleaved by milling of wood,[7,48] and therefore they were still present after milling. The polymeric network of hemicellulose and lignin, connected by the LCCs, hindered the availability of the hydroxy groups of cellulose under our experimental conditions. This led to a slower derivatization process by HMDS, favoring secondary reactions and the observed decrease in the anhydrosugar yield.

The residence time of the pyrolysis products in the furnace is also an important factor to be considered. Longer residence times will favor secondary pyrolysis and reduce the abundance of anhydrosugars in favor of smaller compounds.[38] The average residence time of the pyrolysis products inside the micro-furnace is approximately 10 s. This time is longer than that required for the pyrolysis reaction, which is around 2 s for wood-based samples.[49,50] The presence of the lignin-hemicellulose network in wood likely favored an increase in the residence time of the pyrolysis products of cellulose in the furnace, further favoring secondary pyrolysis. The decrease in the anhydrosugar area after milling was observed mainly for fir and chestnut, which were the wood species that were most affected by this pretreatment.

Contrary to milled samples, the degradation of lignin in irradiated samples most likely led to the cleavage of LCC bonds. In this case, the availability of both cellulose and hemicellulose increased, leading to a more efficient derivatization process upon pyrolysis, and therefore to an increase in the yield of anhydrosugars. The increase in anhydrosugars after milling was in fact mostly observed for the two softwoods, which have a higher lignin content and consequently a higher content of LCCs.[7]

Regarding the lignin fraction, both milling and irradiation led to an increase in the S/P compared to the untreated samples, mainly due to a decrease in the pyrolytic yields of lignin monomers. As expected, these changes were more significant after irradiation, when the integrity of the lignin fraction was affected the most. Irradiated samples also showed significantly higher yields of oxidized lignin pyrolysis products, indicating that irradiation favored not only the release of carbon dioxide, but also the formation of oxidized functional groups.

4. CONCLUSIONS

Milling led to a complete cleavage of the crystalline phase of all wood samples, while irradiation had no significant effect on cellulose crystallinity. The influence of milling on the thermal stability of wood was less significant than what is described in the literature for pure cellulose. Of all the wood species, only fir showed a significant decrease in the apparent activation energy after milling. This result was attributed to the presence of a lower limit in the effectiveness of this pretreatment. While the composition of the substrate plays a fundamental role in determining its thermochemical behavior, the results did not allow detecting clear behavioral schemes among the samples. Further research is required to pinpoint additional factors correlated with the thermal stability of wood and improve our understanding of the energy economy of milled wood.

While the crystalline phase was destroyed by milling, the reactivity of the hydroxy groups of holocellulose toward derivatization did not increase. This led to an increase in the yields of secondary pyrolysis products. Again, this result shows that the advantages of milling as a pretreatment strategy could not be as significant for wood as for isolated cellulose.

Irradiation showed a more significant effect on softwoods than on hardwoods. The effect was mostly registered on the pyrolytic behavior of wood, rather than on its thermal stability. Irradiation caused a reduction in the lignin content of the four investigated species, and an increase in the oxygen content of the lignin fraction. The reduction in the lignin content is a promising feature of UV irradiation, as it increases the availability of holocellulose. Moreover, the increase in the oxygen content after irradiation, and the consequent changes in category areas, suggest that UV irradiation could favor the production of specific valuable chemicals from biomass processing.

https://doi.org/10.1021/acs.energyfuels.1c01048
Energy Fuels 2021, 35, 11353−11365

A controlled UV irradiation of lignocellulosic feedstocks would be difficult to implement on large-scale processing systems. For this reason, UV irradiation could be more suited for laboratory and bench-scale systems. However, the significant effects of photodegradation on the pyrolytic behavior of wood indicate that the exposure of biomass to natural UV should be considered when planning harvesting and storage methods even in large-scale systems.

The results of the present work highlight the potential of EGA-MS and Py-GC-MS in monitoring changes in the thermochemical behavior of wood after both mechanical and physicochemical pretreatments. The results also point out that the same pretreatment method on different wood species can have significantly different effects. Therefore, pretreatment strategies should be carefully optimized in the development of biomass-processing methods both on the laboratory and the industrial scale.

■ ASSOCIATED CONTENT

Supporting Information

The Supporting Information is available free of charge at https://pubs.acs.org/doi/10.1021/acs.energyfuels.1c01048.

XRD spectra; EGA profiles; KAS plots; activation energy-conversion plots; and Py-GC/MS profiles of the samples (PDF)

■ AUTHOR INFORMATION

Corresponding Author

Marco Mattonai − *Department of Chemistry and Industrial Chemistry, University of Pisa, 56124 Pisa, Italy;* orcid.org/0000-0001-5874-1811; Email: marco.mattonai@dcci.unipi.it

Authors

Federica Nardella − *Department of Chemistry and Industrial Chemistry, University of Pisa, 56124 Pisa, Italy*

Luca Zaccaroni − *Department of Chemistry and Industrial Chemistry, University of Pisa, 56124 Pisa, Italy*

Erika Ribechini − *Department of Chemistry and Industrial Chemistry, University of Pisa, 56124 Pisa, Italy*

Complete contact information is available at: https://pubs.acs.org/10.1021/acs.energyfuels.1c01048

Author Contributions

This manuscript was written through contributions of all authors. All authors have given approval to the final version of the manuscript.

Notes

The authors declare no competing financial interest.

■ ACKNOWLEDGMENTS

The Authors would like to acknowledge Dr. Laura De Dosso at the Department of Earth Sciences of the University of Pisa for the XRD experiments. The Authors acknowledge the JPI-Cultural Heritage project "StAr—Development of Storage and Assessment methods suited for organic Archaeological artefacts" (2020−2023).

■ REFERENCES

(1) Wang, S.; Dai, G.; Yang, H.; Luo, Z. Lignocellulosic biomass pyrolysis mechanism: A state-of-the-art review. *Prog. Energy Combust. Sci.* **2017**, *62*, 33−86.

(2) Lin, C.-Y.; Lu, C. Development perspectives of promising lignocellulose feedstocks for production of advanced generation biofuels: A review. *Renewable Sustainable Energy Rev.* **2021**, *136*, 110445.

(3) Wang, Z.; Burra, K. G.; Lei, T.; Gupta, A. K. Co-pyrolysis of waste plastic and solid biomass for synergistic production of biofuels and chemicals-A review. *Prog. Energy Combust. Sci.* **2021**, *84*, 100899.

(4) Schutyser, W.; Renders, T.; Van den Bosch, S.; Koelewijn, S.-F.; Beckham, G. T.; Sels, B. F. Chemicals from lignin: an interplay of lignocellulose fractionation, depolymerisation, and upgrading. *Chem. Soc. Rev.* **2018**, *47*, 852−908.

(5) Beckham, G. T.; Bozell, J.; Houtman, C.; Felby, C.; Rinaldi, R.; Zhang, X.; Bruijnincx, P.; Martinez, A.; Masai, E.; Neidle, E. *Lignin Valorization: Emerging Approaches*; Royal Society of Chemistry, 2018; Vol. *21*.

(6) Mattonai, M.; Pawcenis, D.; del Seppia, S.; Łojewska, J.; Ribechini, E. Effect of ball-milling on crystallinity index, degree of polymerization and thermal stability of cellulose. *Bioresour. Technol.* **2018**, *270*, 270−277.

(7) Tarasov, D.; Leitch, M.; Fatehi, P. Lignin−carbohydrate complexes: properties, applications, analyses, and methods of extraction: a review. *Biotechnol. Biofuels* **2018**, *11*, 269.

(8) Li, M.; Pu, Y.; Ragauskas, A. J. Current Understanding of the Correlation of Lignin Structure with Biomass Recalcitrance. *Front. Chem.* **2016**, *4*, 45.

(9) Yoo, C. G.; Meng, X.; Pu, Y.; Ragauskas, A. J. The critical role of lignin in lignocellulosic biomass conversion and recent pretreatment strategies: A comprehensive review. *Bioresour. Technol.* **2020**, *301*, 122784.

(10) Sankaran, R.; Parra Cruz, R. A.; Pakalapati, H.; Show, P. L.; Ling, T. C.; Chen, W.-H.; Tao, Y. Recent advances in the pretreatment of microalgal and lignocellulosic biomass: A comprehensive review. *Bioresour. Technol.* **2020**, *298*, 122476.

(11) Chaturvedi, V.; Verma, P. An overview of key pretreatment processes employed for bioconversion of lignocellulosic biomass into biofuels and value added products. *3 Biotech* **2013**, *3*, 415−431.

(12) Cardona, C. A.; Quintero, J. A.; Paz, I. C. Production of bioethanol from sugarcane bagasse: Status and perspectives. *Bioresour. Technol.* **2010**, *101*, 4754−4766.

(13) Soltanian, S.; Aghbashlo, M.; Almasi, F.; Hosseinzadeh-Bandbafha, H.; Nizami, A.-S.; Ok, Y. S.; Lam, S. S.; Tabatabaei, M. A critical review of the effects of pretreatment methods on the exergetic aspects of lignocellulosic biofuels. *Energy Convers. Manage.* **2020**, *212*, 112792.

(14) Haldar, D.; Purkait, M. K. A review on the environment-friendly emerging techniques for pretreatment of lignocellulosic biomass: Mechanistic insight and advancements. *Chemosphere* **2021**, *264*, 128523.

(15) Sarkar, N.; Ghosh, S. K.; Bannerjee, S.; Aikat, K. Bioethanol production from agricultural wastes: An overview. *Renewable Energy* **2012**, *37*, 19−27.

(16) Liu, H.; Chen, X.; Ji, G.; Yu, H.; Gao, C.; Han, L.; Xiao, W. Mechanochemical deconstruction of lignocellulosic cell wall polymers with ball-milling. *Bioresour. Technol.* **2019**, *286*, 121364.

(17) Wang, J.; Minami, E.; Asmadi, M.; Kawamoto, H. Thermal degradation of hemicellulose and cellulose in ball-milled cedar and beech wood. *J. Wood Sci.* **2021**, *67*, 32.

(18) Flores, E. M. M.; Cravotto, G.; Bizzi, C. A.; Santos, D.; Iop, G. D. Ultrasound-assisted biomass valorization to industrial interesting products: state-of-the-art, perspectives and challenges. *Ultrason. Sonochem.* **2021**, *72*, 105455.

(19) Luo, J.; Fang, Z.; Smith, R. L., Jr. Ultrasound-enhanced conversion of biomass to biofuels. *Prog. Energy Combust. Sci. Technol.* **2014**, *41*, 56−93.

(20) Mattonai, M.; Watanabe, A.; Shiono, A.; Ribechini, E. Degradation of wood by UV light: A study by EGA-MS and Py-GC/MS with on line irradiation system. *J. Anal. Appl. Pyrolysis* **2019**, *139*, 224−232.

(21) Austin, A. T.; Méndez, M. S.; Ballaré, C. L. Photodegradation alleviates the lignin bottleneck for carbon turnover in terrestrial ecosystems. *Proc. Natl. Acad. Sci. U.S.A.* **2016**, *113*, 4392−4397.
(22) Popescu, C.-M.; Demco, D. E.; Möller, M. Assessment of historic Tilia codrata wood by solid-state 13C CPMAS NMR spectroscopy. *Polym. Degrad. Stab.* **2013**, *98*, 2730−2734.
(23) Baur, S. I.; Easteal, A. J. ESR studies on the free radical generation in wood by irradiation with selected sources from UV to IR wavelength regions. *Holzforschung* **2014**, *68*, 775−780.
(24) Galletti, A. R.; Antonetti, C. Biomass pretreatment: separation of cellulose, hemicellulose, and lignin-existing technologies and perspectives. *Biorefinery: From Biomass to Chemicals and Fuels*; Walter de Gruyter, 2012; pp 101−121.
(25) SriBala, G.; Carstensen, H.-H.; Van Geem, K. M.; Marin, G. B. Measuring biomass fast pyrolysis kinetics: State of the art. *Wiley Interdiscip. Rev.: Energy Environ.* **2019**, *8*, No. e326.
(26) Wang, Y.; Han, Y.; Hu, W.; Fu, D.; Wang, G. Analytical strategies for chemical characterization of bio-oil. *J. Sep. Sci.* **2020**, *43*, 360−371.
(27) Lupoi, J. S.; Singh, S.; Parthasarathi, R.; Simmons, B. A.; Henry, R. J. Recent innovations in analytical methods for the qualitative and quantitative assessment of lignin. *Renewable Sustainable Energy Rev.* **2015**, *49*, 871−906.
(28) Anca-Couce, A. Reaction mechanisms and multi-scale modelling of lignocellulosic biomass pyrolysis. *Prog. Energy Combust. Sci.* **2016**, *53*, 41−79.
(29) Risoluti, R.; Materazzi, S. Mass spectrometry for evolved gas analysis: An update. *Appl. Spectrosc. Rev.* **2019**, *54*, 87−116.
(30) Nardella, F.; Mattonai, M.; Ribechini, E. Evolved gas analysis-mass spectrometry and isoconversional methods for the estimation of component-specific kinetic data in wood pyrolysis. *J. Anal. Appl. Pyrolysis* **2020**, *145*, 104725.
(31) Park, S.; Baker, J.; Himmel, M.; Parilla, P.; Johnson, D. Cellulose crystallinity index: measurement techniques and their impact on interpreting cellulase performance. *Biotechnol. Biofuels* **2010**, *3*, 10.
(32) French, A. D. Idealized powder diffraction patterns for cellulose polymorphs. *Cellulose* **2014**, *21*, 885−896.
(33) Yue, Y.; Han, J.; Han, G.; Zhang, Q.; French, A. D.; Wu, Q. Characterization of cellulose I/II hybrid fibers isolated from energycane bagasse during the delignification process: Morphology, crystallinity and percentage estimation. *Carbohydr. Polym.* **2015**, *133*, 438−447.
(34) Joseph, A.; Bernardes, C. E. S.; Druzhinina, A. I.; Varushchenko, R. M.; Nguyen, T. Y.; Emmerling, F.; Yuan, L.; Dupray, V.; Coquerel, G.; da Piedade, M. E. M. Polymorphic Phase Transition in 4′-Hydroxyacetophenone: Equilibrium Temperature, Kinetic Barrier, and the Relative Stability of Z′ = 1 and Z′ = 2 Forms. *Cryst. Growth Des.* **2017**, *17*, 1918−1932.
(35) Mattonai, M.; Tamburini, D.; Colombini, M. P.; Ribechini, E. Timing in Analytical Pyrolysis: Py(HMDS)-GC/MS of Glucose and Cellulose Using Online Micro Reaction Sampler. *Anal. Chem.* **2016**, *88*, 9318−9325.
(36) Fabbri, D.; Chiavari, G. Analytical pyrolysis of carbohydrates in the presence of hexamethyldisilazane. *Anal. Chim. Acta* **2001**, *449*, 271−280.
(37) Tamburini, D.; Łucejko, J. J.; Zborowska, M.; Modugno, F.; Prądzyński, W.; Colombini, M. P. Archaeological wood degradation at the site of Biskupin (Poland): wet chemical analysis and evaluation of specific Py-GC/MS profiles. *J. Anal. Appl. Pyrolysis* **2015**, *115*, 7−15.
(38) Mamleev, V.; Bourbigot, S.; Le Bras, M.; Yvon, J. The facts and hypotheses relating to the phenomenological model of cellulose pyrolysis: Interdependence of the steps. *J. Anal. Appl. Pyrolysis* **2009**, *84*, 1−17.
(39) Moldoveanu, S. C. *Pyrolysis of Organic Molecules: Applications to Health and Environmental Issues*; Elsevier, 2009; Vol. *28*, pp 419−447.
(40) Paine, J. B.; Pithawalla, Y. B.; Naworal, J. D. Carbohydrate pyrolysis mechanisms from isotopic labeling. Part 5. The pyrolysis of D-glucose: The origin of the light gases from the D-glucose molecule. *J. Anal. Appl. Pyrolysis* **2019**, *138*, 70−93.
(41) Shen, D. K.; Gu, S.; Luo, K. H.; Wang, S. R.; Fang, M. X. The pyrolytic degradation of wood-derived lignin from pulping process. *Bioresour. Technol.* **2010**, *101*, 6136−6146.
(42) González-Vila, F. J.; González-Pérez, J. A.; Akdi, K.; Gómis, M. D.; Pérez-Barrera, F.; Verdejo, T. Assessing the efficiency of urban waste biocomposting by analytical pyrolysis (Py−GC/MS). *Bioresour. Technol.* **2009**, *100*, 1304−1309.
(43) Popescu, C.-M.; Singurel, G.; Popescu, M.-C.; Vasile, C.; Argyropoulos, D. S.; Willför, S. Vibrational spectroscopy and X-ray diffraction methods to establish the differences between hardwood and softwood. *Carbohydr. Polym.* **2009**, *77*, 851−857.
(44) Tamburini, D.; Łucejko, J. J.; Ribechini, E.; Colombini, M. P. Snapshots of lignin oxidation and depolymerization in archaeological wood: an EGA-MS study. *J. Mass Spectrom.* **2015**, *50*, 1103−1113.
(45) Schmatz, A. A.; Tyhoda, L.; Brienzo, M. Sugarcane biomass conversion influenced by lignin. *Biofuels, Bioprod. Biorefin.* **2020**, *14*, 469−480.
(46) Mattonai, M.; Ribechini, E. Pyrolysate composition and silylation efficiency in analytical pyrolysis of glucans as a function of pyrolysis time. *J. Anal. Appl. Pyrolysis* **2020**, *145*, 104747.
(47) Zhao, Y.; Shakeel, U.; Saif Ur Rehman, M.; Li, H.; Xu, X.; Xu, J. Lignin-carbohydrate complexes (LCCs) and its role in biorefinery. *J. Cleaner Prod.* **2020**, *253*, 120076.
(48) Balakshin, M.; Capanema, E.; Berlin, A. Chapter 4 - Isolation and Analysis of Lignin−Carbohydrate Complexes Preparations with Traditional and Advanced Methods: A Review. In *Studies in Natural Products Chemistry*; Atta ur, R., Ed.; Elsevier, 2014; Vol. *42*, pp 83−115.
(49) Van de Velden, M.; Baeyens, J.; Brems, A.; Janssens, B.; Dewil, R. Fundamentals, kinetics and endothermicity of the biomass pyrolysis reaction. *Renewable Energy* **2010**, *35*, 232−242.
(50) Proano-Aviles, J.; Lindstrom, J. K.; Johnston, P. A.; Brown, R. C. Heat and Mass Transfer Effects in a Furnace-Based Micro-pyrolyzer. *Energy Technol.* **2017**, *5*, 189−195.

https://doi.org/10.1021/acs.energyfuels.1c01048
Energy Fuels 2021, 35, 11353−11365